OPEN

Correspondence and
requests for materials
should be addressed to
S.C.R. (Raysc@unisa.
ac.za)

* Current address:
Institute of Renewable
Energy and
Environmental
Technologies (IREET),
Knowledge Centre for
Materials Chemistry
(KCMC) University of
Bolton, Deane Road,
Bolton BL3 5AB, United
Kingdom.

Graphene Supported Graphone/Graphane Bilayer Nanostructure Material for Spintronics

Sekhar C. Ray[1], Navneet Soin[2]*, Thuto Makgato[3], C. H. Chuang[4], W. F. Pong[4], Susanta S. Roy[5], Sarit K. Ghosh[6], André M. Strydom[6,7] & J. A. McLaughlin[2]

[1]Department of Physics, College of Science, Engineering and Technology, University of South Africa, Private Bag X6, Florida, 1710, Science Campus, Christiaan de Wet and Pioneer Avenue, Florida Park, Johannesburg, South Africa, [2]Nanotechnology and Integrated Bioengineering Center (NIBEC), School of Engineering, University of Ulster, Jordanstown campus, Newtownabbey, BT37 0QB, United Kingdom, [3]Department of Physics, University of the Witwatersrand, Johannesburg, South Africa, [4]Department of Physics, Tamkang University, Tamsui 251, Taipei, Taiwan, [5]Department of Physics, School of Natural Sciences, Shiv Nadar University, Gautam Budh Nagar 203207, UP, India, [6]Department of Physics, University of Johannesburg, PO Box 524, Auckland Park 2006, South Africa, [7]Max Planck Institute for Chemical Physics of Solids, Nöthnitzerstr, 40, 01187 Dresden, Germany.

We report an investigation into the magnetic and electronic properties of partially hydrogenated vertically aligned few layers graphene (FLG) synthesized by microwave plasma enhanced chemical vapor deposition. The FLG samples are hydrogenated at different substrate temperatures to alter the degree of hydrogenation and their depth profile. The unique morphology of the structure gives rise to a unique geometry in which graphane/graphone is supported by graphene layers in the bulk, which is very different from other widely studied structures such as one-dimensional nanoribbons. Synchrotron based x-ray absorption fine structure spectroscopy measurements have been used to investigate the electronic structure and the underlying hydrogenation mechanism responsible for the magnetic properties. While ferromagnetic interactions seem to be predominant, the presence of antiferromagnetic interaction was also observed. Free spins available via the conversion of sp^2 to sp^3 hybridized structures, and the possibility of unpaired electrons from defects induced upon hydrogenation are thought to be likely mechanisms for the observed ferromagnetic orders.

Graphene composed of a single-atomic layer of carbon atoms has emerged as fascinating example of designer materials, where dimensionality plays an important role and it has become a novel platform for the engineering of novel electronic and magnetic-storage devices[1–6]. For spintronic applications, graphene is considered as a promising material due to its long spin relaxation time and length because of the small spin-orbit coupling of carbon atoms[5,6]. Similar to the modulation of physical and chemical properties of carbon nanotubes, various strategies for modulating the electronic and magnetic properties of graphene have been proposed for versatile applications[7–9]. Sofo et al predicted that fully hydrogenated graphene (*graphane*) could be a non-magnetic semiconductor with a band gap of 4.5 eV, which was later confirmed experimentally[7,8]. Zhou et al predicted that semi-hydrogenated graphene sheet (graphone) can become ferromagnetic at room temperature with a band gap of 0.46 eV, which is much smaller than that of graphane (4.5 eV)[9]. This change in the band gap occurs via the formation of tetrahedral carbon (ta-C), which reduces the connectivity of the π-sheets of graphene and the $\pi - \pi$ energy gap of the localized double bonds (i.e. the formation of an alternating sp^2–sp^3–sp^2–sp^3 hybridization pattern). Furthermore, calculations have also shown that hydrogen pairs arranged in lines can create semiconducting or metallic waveguides through confinement effects. A large band gap opening in hydrogen-covered regions would lead to an effective potential barrier for the electrons. Experimentally, disordered hydrogen adsorption has been shown to influence the transport properties in graphene through localization effects[10], which may occur due to adsorption of hydrogen on free-standing graphene[11], as well as on supported graphene layer[12,13]. Zhou et al predicted that in semi-hydrogenated bi-layer graphene (referred as BL-graphone), the most stable configuration undergoes a (1×2) surface reconstruction[14]. The graphone (partial hydrogenation) sheet can be synthesized by supporting graphene first on a substrate followed by a hydrogenation process; otherwise removing of half of the hydrogen atoms from one surface of graphane[9,15]. In this (*graphone*) process, the graphene leads to the formation of unpaired electrons and the remanent delocalized bonding network which is responsible for the formation of ferromagnetic materials with Curie temperatures between 278 K to 417 K and

could be most promising materials for future spintronics applications[9,16]. Since graphene, graphane and graphone individually show remarkable properties and are expected to have versatile electronic and magnetic device applications, it is a compelling study to investigate the electronic structure and magnetic properties when two of them bind each other like graphene-graphane and graphene-graphone bilayer structures. Remarkable properties extend to bilayer and few-layers graphene and even combination of graphene and graphone layers[14]. When graphene and graphone both in single layer sheet bind together, metallic but nonmagnetic characteristics are formed as predicted theoretically by Zhou et al[14]. They show that two pristine graphene sheets cannot be bonded together due to the prevailing weak van der Waals interaction. But, in presence of H the unsaturated C sites in the graphone sheet are reactive because of unpaired electrons. A graphene sheet can bind to graphone and the system can be viewed as semi-hydrogenated bi-layer graphene (BL-graphone) or simply graphene supported graphone[14]. Furthermore at the interface between graphene and graphane, magnetism arising from the edges can be tuned[17].

In this work, we have studied the graphene supported graphone/graphane bilayer structure to elucidate their electronic structure and magnetic behaviors with a view on spintronics applications. The magnetism in carbon-based materials is quite unique in itself as it arises from only s and p orbital electrons unlike the magnetism, which arises more intuitively from the 3d or 4f electrons in traditional magnetic materials. Using microwave plasma enhanced chemical vapor deposition, thin vertically aligned few layers graphene (FLG) nanoflakes were synthesized on bare Si(100) substrates, which were further subjected to hydrogen plasma treatment. The FLG samples are hydrogenated at different substrate temperatures to alter the hydrogenation depth and process. The particular morphology of the structures gives rise to a unique geometry in which graphane/graphone layers are supported by graphene layers in the bulk which is very different from other more widely studied structures such as one-dimensional nanoribbons. The change in the electronic and magnetic properties was measured as a function of hydrogen content introduced in the structures and its temperature dependence using X-ray absorption, Raman spectroscopy and magnetic force microscopy. Field-dependent magnetization of representative samples was studied using a SQUID-type magnetometer. The work provides further knowledge and contributions to the emerging body of experimental and theoretical data related to magnetism in graphene and graphene based nanostructures.

Results and discussion

The scanning electron microscopy (SEM) images of pristine and hydrogenated few layers graphene (FLG:H) are shown in Fig. 1(a, b) and it is evident that the synthesized FLG are vertically aligned to the underlying substrate and are randomly intercalated to each other forming a porous mesh-like network. The H_2 plasma treatment process does not disturb the vertically aligned nature of the graphene platelets; however it leads to an increase in the sharp graphene edges throughout the sample. Also, it is found that the apparent thickness of the edges of graphene platelets is reduced due to plasma etching effects. Figure 1(c) plots the electron field emission (EFE) current density (J) as a function of the applied electric field (E_A). The figure shows that there exists a threshold of electric field, beyond which J increases roughly exponentially. Fowler-Nordheim (*F-N*) plots (see supplementary material S1) clearly illustrate the threshold electric field or turn-on electric field (E_{TOE}). The values of E_{TOE} were obtained with linear **in** J-E_A curve fitting in the high electric field region (shown in S1) and were found to increase from 26.5 V/μm (pure FLG) to 36.3 V/μm for FLG:H@50°C (whereas 64.4 V/μm is obtained for FLG:H@200°C) indicating that H-doping promotes the three-dimensional sp^3 bonding configuration[18].

The Raman spectra of pristine FLG and FLG:H treated at different temperatures are shown in Figure 2(a). The Raman spectrum of the pristine FLG displays three characteristic peaks: D band at ~1335 cm^{-1}, G band at ~1583 cm^{-1} and 2D band at ~2664 cm^{-1}. Post hydrogen-plasma treatment, the Raman spectra of the FLG change significantly with the increase in the intensities of peaks at 1617 cm^{-1}, 2462 cm^{-1} and 2920 cm^{-1}. The peaks at ~2460 and 2920 cm^{-1} arise via a combination of (D + D′) bands and are defect activated[19-22]. The D peak too is defect activated via an intervalley double resonance process and its intensity provides a convenient measure for the amount of disorder[19-23]. The D peak is enhanced after hydrogenation and is due to hydrogen attachment, which breaks the translational symmetry of C=C sp^2 bonding[24]. Upon hydrogenation, the 2D band of FLG:H also becomes intense and shows a red-shift accompanied by a change in the I_{2D}/I_G ratio as shown in Fig. 2(b). Now, the position and peak intensities of G and 2D band can be used as a fingerprint for mono, bi-, tri- or
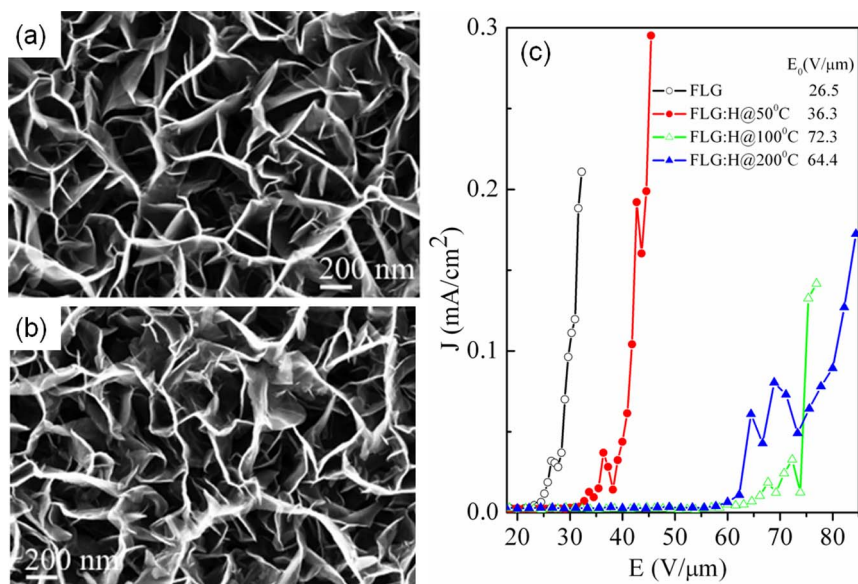

Figure 1 | SEM images of (a) pristine and (b) hydrogenated FLG (FLG:H@50°C) showing the increase in the disorder. (c) Electron Field Emission of FLG and FLG:H.
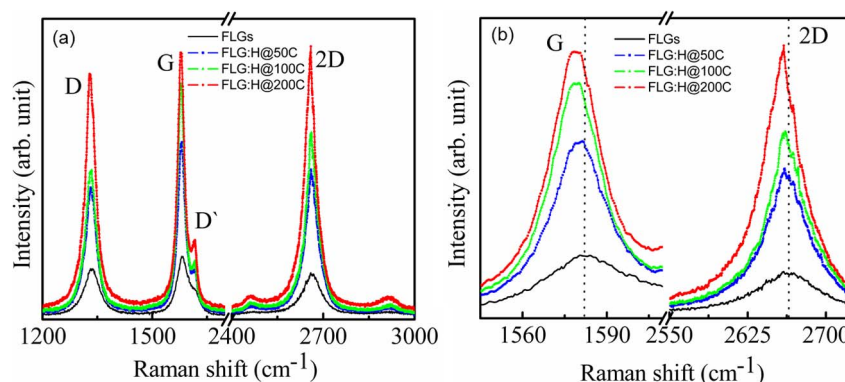
Figure 2 | (a) Raman spectra of pristine and FLG hydrogenated at different temperatures (FLG:H), (b) the red-shift of G and G′ (2D) peaks upon hydrogenation at different temperatures.

multilayered graphene[19]. When compared to pristine FLG, the hydrogenated samples show a shift from 2664 to 2660 cm^{-1}, signifying the formation of bi- or tri- layer grapheme[19,23]. This reduction in the number of graphene-layers is further confirmed from the intensity ratio of the 2D and G peaks. It is observed that the (I_{2D}/I_G) ratio changes from 0.75 (FLG) → 1.1 (FLG:H@50°C) → 0.80 (FLG:H@100°C → 0.85 (FLG:H@200°C). A I_{2D}/I_G ratio of >1 is indicative of the formation of bi-layer graphene, whereas an I_{2D}/I_G ratio of <1 represents tri- or multilayered graphene[24]. The increase in the intensity of D band (at 50°C) along with the presence of a new band observed at ∼1617 cm^{-1} (denoted as D′) can be attributed to the attachment of hydrogen on the top layer or the inter-layer of FLG. As compared to pristine FLG, the FLG:H shows an increase in the intensity of D, 2D and (D + D′) bands owing to the break in the translational symmetry of C=C sp^2 bonds and the formation of C-H sp^3 bonds[22]. The features and peak position of D and 2D of our non-hydrogenated graphene identifies as FLG; whereas hydrogen functionalized graphene (FLG:H) identifies as bi- or tri-layer graphene. Also, with an increase in the hydrogenation temperature, the G-band shifts by ∼3 cm^{-1}, caused by a change in charge density[25,26]. A similar reduction in the number of graphene layers upon hydrogen plasma treatment has been observed elsewhere[27].

Since the FLG are vertically aligned on a Si-substrate, it is expected that only the top-most surfaces of the FLG would be predominantly accessible to atomic hydrogen. At low temperature (50°C in the present case), the hydrogen-plasma exposure is not expected to result in *graphane* where the hydrogen atoms are attached on both sides of the graphene sheet. The microwave plasma system used in this work is operated at a moderate pressure (2 Torr) and a relative high power density (14 Wcm^{-3}) as compared to capacitively coupled radio frequency systems (1 Torr/0.03 Wcm^{-3}) used in other studies[16]. At higher temperatures (100°C–200°C) and plasma powers, it can be expected that the various species generated (H^+, H_3^+ and hydrogen radicals) are able to passivate/percolate through the top layer and form C-H bonds with the subsequent underlying graphene layers. Also, at higher temperatures (100°C–200°C) the graphene flakes are functionalized and annealed simultaneously. Luo et al. observed that the annealing process for graphene starts above 75°C and is completed at 350°C with a long annealing duration[28]. If the hydrogenation and annealing are occurring simultaneously at temperatures of the order of 100°C–200°C, then it is expected that C-H bonds will be formed in the inner layers of the FLG, once the top surface of the FLG has been hydrogen passivated. The 2D band of hydrogen functionalized FLG is very sharp, strong and red-shifted compared to pure FLG indicative of the reduction in the number of graphene layers[19,23].

For graphitic materials in general, x-ray absorption near edge structure (XANES) spectra can be divided into three regions characterized by specific resonance energies[29]. The first region of π^*

resonance appears around 285 ± 1 eV, the C-H* resonance around 288 ± 1 eV, and a broad region between 290 eV – 315 eV corresponds to σ^* resonance. The presence of the π^* and C-H* resonances serve as a fingerprint for the existence of sp^2 hybridized C-C bonds and C-H bonds, respectively. The C K-edge XANES spectra of the samples (Figure 3) show features at ∼285.1 (±1) eV, ∼292.6 (±1) eV and ∼291.6 (±1) eV which can be attributed to the unoccupied 1 s → π^*, 1 s → σ^* and excitonic states transitions, respectively[29]. While, the peak positions for FLG:H@50°C are similar to that of pristine FLG, the absorption edges are shifted towards lower energy level for FLG:H@100°C (200°C) [285.3 eV (FLG &
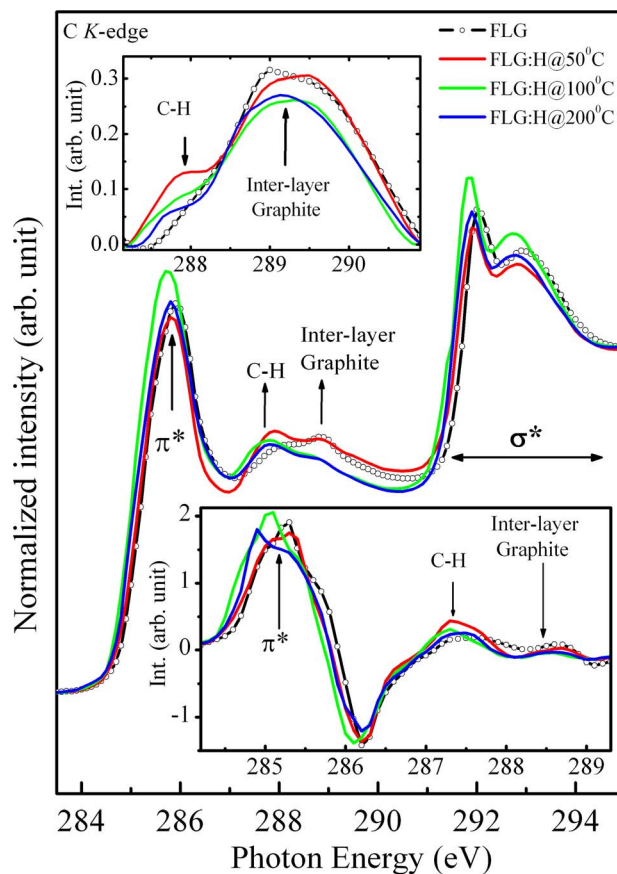

Figure 3 | XANES spectra of pristine and FLG:H samples. The top inset shows the increase in the C-H content whereas the bottom inset shows the first order differential spectrum for the scans (inset below: Green and Blue spectra are shifted by 0.2 eV).

3

FLG:H@50°C) → 285.1 (FLG:H@100°C) → 284.9 eV (FLG:H@ 200°C)] as clearly shown in the first order differential spectrum inset below in figure 3. This change in the absorption edge is attributed to the change in the band gap of FLG:H@100-200°C due to the structural rearrangement via hydrogen attachment[30]. A very low intensity peak is also observed at ~283.3 eV, nearly 2.0 eV lower than the π* state for the FLG:H@50°C as shown in supplementary information S2. While this feature has been observed in graphene samples in the past, the origin of it is still highly debated. Hou et al. and Entani et al. have considered that this peak originates from the zig-zag edge C atoms which have a spin-polarized edge state closed to the Fermi level[30,31]. They have proposed that there is a difference in the 1s core level binding energy between the carbon atom located in the interior of the graphene nano-cluster and one located at the zig-zag edge[30]. Alternatively, Pacile et al have ascribed this shoulder to the splitting of the π* bands in graphene[32]. In the theoretical work by Hua et al, this shoulder has been attributed to a special extended final state or to Stone-Wales defects[33]. As reported by Hou et al., the intensity and the position of this peak strictly depends on hydrogen content as well as the ratio of monohydrogen (-CH) to dihydrogen (-CH₂) terminations in the graphene structure[31]. While monohydrogen termination produces the shoulder at approximately 2–2.5 eV lower than the π* resonance, mono-hydrogen termination is stable only at very low hydrogen partial pressures. Under "standard" conditions, the structures are more likely to be a mixture of mono and dihydrogen terminations along the graphene edges[31]. For our samples, in the case of FLG:H@100°C (200°C) samples the π* peak lies 0.2 eV (0.4 eV) lower compared to FLG:H@50 (inset below in fig. 3), leading to the conclusion that the dihydrogen (-CH₂) termination is increasing with the increase in temperature treatment. It is also possible that are defects being created by the hydrogen plasma treatment. Raman spectra show (Fig. 2) an increase in the defects at 50°C with anomalous behavior at 100°C and 200°C.

Apart from π* and σ* resonance peaks, two other peaks at ~287.4 ± 1 eV and ~288.5 ± 1 eV (inset in top panel of figure 3) are observed and ascribed as signatures of C-H bonds and interlayer graphite states, respectively. When compared to pristine FLG, the FLG:H spectra show an increased intensity of the C-H peak accompanied by a reduction in the interlayer graphite peak intensity. This increase in the C-H peak intensity confirms the formation of sp³-rich structures having a higher content of C-H bonds. We have estimated the C-H content relative to pristine FLG from the C-H peak in C K-edge XANES spectra using a proper baseline corrected curve-fitting procedure (in the range of 287–291 eV), as described in supplementary information S3. It is found that the C-H content decreases from 0.065 → 0.032 → 0.019 (arbitrary units) with an increase in the functionalization temperatures 50 → 100 → 200°C. During functionalization, all process control conditions were kept similar except for the substrate temperature apparently leading to a change in the content of C-H bonds. It is known that with decrease in the hydrogen content the band gap of graphene reduces[34]. However, in our case it is estimated that the band gap actually increases slightly for FLG:H@ 100°C–200°C when compared to pristine FLG and FLG:H@50°C. This can be observed via the shift of the C K-edge towards lower energy levels with the reduction of C-H content (inset below in figure 3,). However, we have attempted to determine the bandgap value with the help of C $K_α$ x-ray emission spectra (XES) and C K-edge XANES spectra[35]. It was observed that the extrapolation of the leading edges of XES and XANES spectra leads to a clear intersection, implying that FLG and FLG:H have a zero band gap, similar to the metallic highly oriented pyrolytic graphite as described in supplementary information S4. Intuitively, one would expect that formation of the sp³ configuration will lead to a change in the band gap such as in graphane (band gap of 3.12 eV). Graphane is a direct gap material for which electron and optical gaps are of similar magnitude, however most of the partially hydrogenated systems

demonstrate an indirect optical band gap[36]. It should be noted that XANES, measured in electron yield mode is a surface sensitive technique with an electron escape depth of ~3–5 nm[29]. As mentioned before, the shift in the absorption edge of the C -K edge spectra leads us to the conclusion that the band gap increases for the FLG:H@ 100°C–200°C as compared to pristine FLG and FLG:H@50°C. Hence, it is important to consider the effect of temperature on the formation and distribution of C-H bonds. It is quite interesting to observe that the estimated C-H content is approximately in the ratio 3 : 1.5 : 1 (≅ 6 : 3 : 2) at 50°C, 100°C and 200°C respectively, indicating the C-H bonds are distributed in three different ways at three different temperatures on the graphene surface. At relatively lower temperatures of 50°C, we can consider the possibility of hydrogenation occurring on only the top-most surface layer of the FLG[37]. At higher temperatures (100°C–200°C), we believe that hydrogen can passivate the surface as well as to form C-H bonds in the inner-layers of FLG, which may not be detected by XANES due to the electron escape depth limitation. The hydrogenation can occur in the inner-layers of FLG only after overcoming the energy barrier to penetrate the centre of the hexagonal bonded carbon in the top-most surface layer[38]. Hence, the C-H contents observed and measured in the XANES spectra are lower at 100°C–200°C temperatures. Under the same hydrogenation conditions except temperature, the different hydrogen coverage on first layer and second layer indicates that the corresponding hydrogenation barriers differ from each other. Based on the, hydrogenation and C-H bond formation in FLG at different functionalization temperatures, we may consider the formation of graphene supported graphone/graphane bi- or tri-layer nanostructure materials. Again, Raman spectra show that the I_D/I_G ratio is decreased for the H-functionalized FLG at 100–200°C temperature compared to FLG:H@50°C, suggesting that a slow de-hydrogenation process may also have occurred along with hydrogenation process in the H₂-plasma atmosphere. This could be another reason for the lower content of C-H bonds present in FLG:H functionalized at 100 and 200°C. In our studies, the hydrogenation process is carried out for a 90 second duration only, thus avoiding the consequences of long annealing duration as described by Luo et al[28]. So, the effect of de-hydrogenation should ideally be low, leading to the conclusion that at higher temperatures, the surface passivation is followed by the penetration of "top-most" graphene layer to form C-H bonding in the inner-layers of the FLG. Based on the formation of this graphene supported graphone/graphane bi-/tri-layer nano-structure materials we have studied the magnetic behaviors of these materials.

The magnetic properties of the FLG and FLG:H samples were measured in the range of −2 kOe < H < 2 kOe at temperatures of 300 K and 40 K, respectively. The measured magnetic hysteresis loops are shown in Figure 4, with the FLG:H@50°C sample showing the most expressed ferromagnetic behavior with maximum field hysteretic features and highest saturation moments (Ms = 13.94 × 10⁻⁴ emu/gm), while other samples show more confined hysteretic features and lower saturation moment (see Table 1). As compared to pristine FLG, the magnetic moment values of FLG:H@100°C (see supplementary information S5) and FLG:H@200°C are slightly higher due to hydrogen incorporation in the FLG resulting in the formation of sp³ hybridized carbon structure through mono- and possible di-hydrogen termination. Since the FLG samples are free from any catalyst remnants and detectable foreign magnetic impurities (see XPS supplementary information S6), the observed magnetism in the samples can be attributed to (i) defects and vacancies created during synthesis, and (ii) creation of sp³ hybridised structures[39–41]. The I_D/I_G ratio trend of pristine and hydrogenated FLG (Figure 2) shows that the FLG:H@50°C samples have the highest defect ratio along with the highest content of hydrogen as measured from XANES. Thus, the FLG:H@50°C samples are expected and indeed do show the highest magnetization signals. As discussed before, at the relatively lower temperatures of 50°C, the
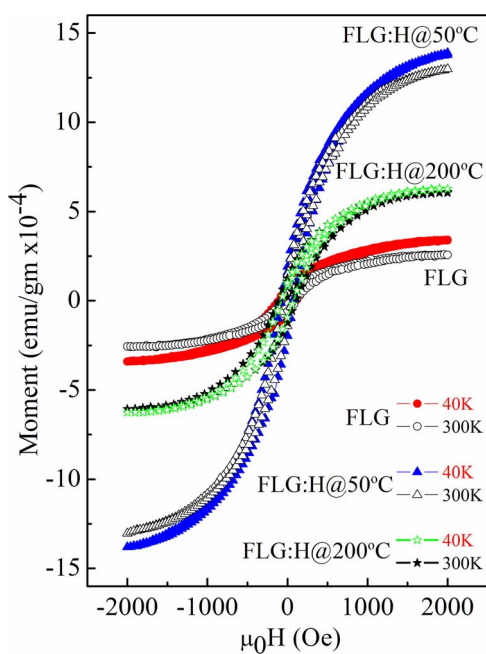
Figure 4 | Magnetic hysteresis loops obtained for FLG and FLG:H samples at 300 K and 40 K, respectively.

hydrogenation may possibly occur on only the top-most surface layer of the FLG; thereby favoring the higher observed magnetic moment[37]. Similar to the results reported by others, we observed maxima in the magnetization at lower temperatures especially for FLG:H@50°C sample (see supplementary information S7)[42]. Based on different hydrogen attachment on graphene (see schematic view in supplementary information S8) Yazyey et al. predicted[43] that the ortho-dimers and para-dimers are nonmagnetic; while single hydrogen attachment (monomer) to be magnetic[16]. This may explain why FLG:H@50°C is more magnetic than FLG:H@100°C (200°C).

Since the magnetism observed in FLG:H is attributed to an intrinsic mechanism beyond reasonable doubt, it is important to discuss the role of hydrogen in enhancing the magnetism in nanostructured carbon and how it can be promoted during the synthesis itself. It has been shown theoretically that hydrogenation is an efficient way in which to introduce and enhance magnetism in graphene sheets. The addition of hydrogen leads to the rupturing of the delocalised π bonding network of graphene, leaving the $2p_z$ electrons in the un-hydrogenated carbon atoms unpaired, and thereby extending the p-p interactions resulting in the long-range ferromagnetic coupling with a putative higher Curie temperature and a more homogeneous magnetism[44,45]. Now, similar to the functionalisation strategies of other nanomaterials, the synthesis of hydrogenated graphene can be done via either a wet chemistry route or by plasma-based processes. The wet chemistry approach includes solution based Birch reduction of graphite oxide to yield graphane or by liquid phase hydrogenation/exfoliation of graphite[46,47]. The plasma functionalization route involves hydrogenation of sp² carbon materials such as CNTs, graphene or graphene oxide in a hydrogen gas/plasma environment[47]. Arc-discharge of graphite in a hydrogen rich environment

has also been shown as an effective method for the synthesis of graphene[48]. However, theoretical calculations have suggested that the formation of graphene via hydrogenation of graphene will not yield large graphitic domains, since uncorrelated H frustrated domains are expected to be formed during the early stages of hydrogenation reaction[47]. This will invariably lead to the shrinkage of the graphene sheet leading to extensive sheet corrugations; thus making the direct deposition of graphane more desirable[47]. Zhou et al have proposed a physical method to fabricate a semi-hydrogenated graphene sheet[45]. Their idea revolves around the use of graphane as a substrate to support the Boron nitride sheet, after which the BN sheet is fluorinated. As the binding of the F with N is highly unstable, the F-BN configuration can be easily achieved. Due to the presence of unpaired electrons, the N atoms are quite reactive in nature and upon the application of pressure, will pick up the H atoms from graphane. When the applied pressure is removed, the resultant structure is semi-hydrogenated in nature[45]. In our case, since we are depositing FLG from the gas phase in plasma, the direct deposition of hydrogenated graphene *via* plasma deposition similar to work reported by Wang et al can be a feasible route for enhancing the magnetic properties of FLG during the synthesis itself[49]. The process reported by Wang et al involves the use of remote discharged 13.5 MHz radio-frequency plasma inside an ultra-high vacuum source[49]. The pre-cracking of the gaseous precursors to generate the reactive free radicals in gas phase allows for lower substrate temperatures and also limits the damage caused by energetic plasma ions during the growth of film. The growth process was carried out using a premixed 5% CH_4 in H_2, resulting in an excess of atomic hydrogen in the gas phase and the inevitable hydrogenation of graphene films with formation of graphane[49]. In literature, the role of hydrogen during the non-catalytic growth of FLG has been linked to the etching of amorphous carbon films which may occur during the initial nucleation stages[50,51]. Thus, for the formation of magnetic graphene structures, careful tuning of plasma parameters such as gas conditions, plasma power, temperature, ion energy and bias in the microwave plasma will be required. The ferromagnetic order arises from the free spins available via the conversion of sp² to sp³ hybridised structures and/or from the unpaired spin electron from the defects induced upon hydrogenation[52]. Both these factors may in principle be responsible for producing fundamental magnetic species. The ferromagnetic ordering of the spins is energetically preferable for the AA distribution in the graphene plane. Therefore, it can be stated that the ferromagnetic exchange of spins of the localized states in graphane is possible only among the H-vacancy defects located on the exchange neighboring carbon atoms[53,54]. Defects in our bi-/tri-layer graphene break the translational symmetry of the lattice and create localized states at the Fermi energy to produce an effective self-doping, where charge is transferred from defects to the bulk. In the presence of local electron-electron interactions, these localized states become spin-polarized, leading to the formation of pseudo-local moments[55]. Most of the theoretical[41,56–58] and experimental[56,57] works find that the net spin is stable within a large conjugation system in unit structures of graphene at room temperature and their stability is due to the huge π-conjugation in these molecules. If indeed the long-range orderly magnetic coupling of these spins may arise via either intra-molecular interaction in individual graphene sheets or inter-molecular interaction between neighboring graphene sheets, then stable ferromagnetism could arise[41]. We agree that the room-temperature ferromagnetism is an intrinsic property of graphene-based materials, and for direct and conclusive evidence we have performed further magnetic force microscopy (MFM) analysis.

Low moment magnetic probes with Co/Cr coating were used to detect magnetic domains in the pristine and hydrogenated FLG samples. Figure 5–6 shows topographic (height), amplitude and phase signals were imaged simultaneously for both tapping mode AFM (TM-AFM) and MFM to assess correlation of surface features,

Table 1 | Magnetization parameters of FLGs and FLGs:H

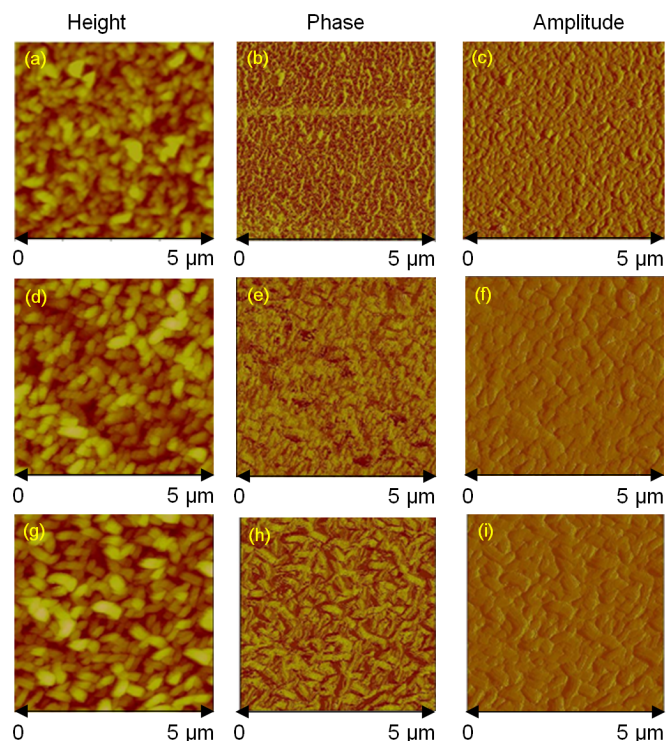| Sample	M_S (emu/gm $\times 10^{-4}$)		H_C (Oe)	
	40 K	300 K	40 K	300 K
Pristine FLGs	3.47	2.59	111.25	82.63
FLG:H@50C	13.94	12.91	75.32	54.36
FLG:H@200C	6.10	6.40	76.15	110.06

Figure 5 | Atomic Force Microscopy images of pristine (a–c) and hydrogenated FLG [(d–f) @ 50°C and (g–i) @200°C].

identify and eliminate possible artifacts and to assess effects of magnetization. The magnetized Co/Cr coated probe interacts with magnetic field gradients generated by magnetic domains within the prepared sample resulting in changes in the phase and amplitude of the oscillating cantilever. Therefore, from the amplitude and phase images the existence of magnetic domains in the samples should be evident. The MFM phase and amplitude images show very good
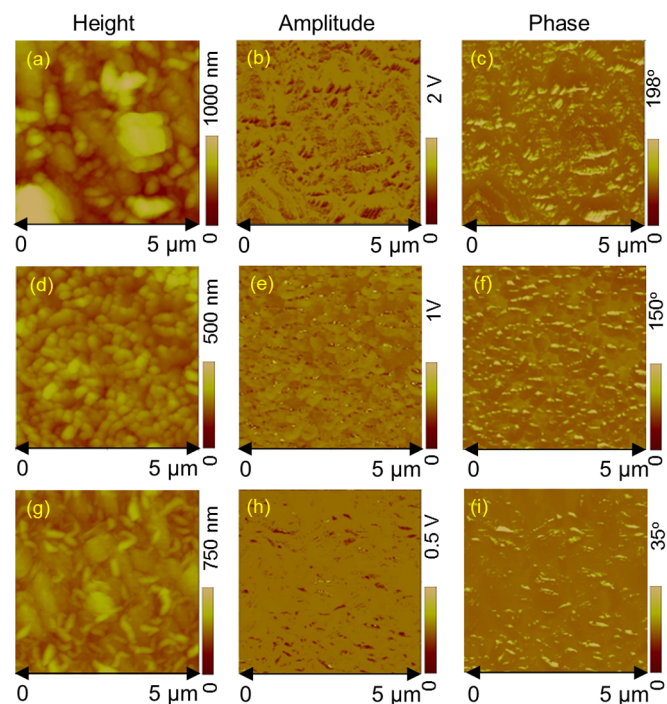

Figure 6 | Magnetic Force Microscopy images of pristine (a–c) and hydrogenated FLG [(d–f) @ 50°C and (g–i) @200°C].

correlation in magnetic domain positions. For all samples, the magnetic domains appear as dark and bright-localized regions in phase and amplitude images respectively. Images clearly show that the domains in the FLG:H are more localized than in the case of FLG. A simple scaling of MFM phase data suggests that pristine FLG has the weakest magnetization, whereas the FLG@50°C the strongest magnetization effect, which is consistent with the M-H magnetization results, described above.

In conclusion, room temperature ferromagnetism was observed in partially hydrogenated graphene. Hydrogenation was confirmed by XANES measurements with the appearance of a C-H resonance peak. The mechanism of the observed ferromagnetism is explained by the formation of unpaired electrons during the hydrogenation process, together with the remnant delocalized π-bonding network existing in the partially hydrogenated graphene. The fabrication of a variety of spintronic devices requires attribution such as ferromagnetic properties together with an electrically semiconducting matrix, prevailing at room temperature. The hydrogenation process is demonstrated in our study to conceivably turn graphene into a robust room-temperature ferromagnetic semiconductor and open up the possibility of producing highly tunable graphene-based applications devices, including spintronic nano-devices, magnetoresistance and magnetic memory devices.

Methods

Preparation of few layer graphene and hydrogen functionalized graphene. The synthesis of FLG was carried out in a SEKI microwave plasma enhanced chemical vapor deposition system, equipped with a 1.5 kW, 2.45 GHz microwave source. The substrates used were bare n-type heavily doped Si wafers (resistivity $<$ 0.005 Ω cm) (10 mm $\times$ 10 mm). Prior to growth, the substrates were pretreated with N_2 plasma at 650 W at 40 Torr while the substrate temperature was maintained at 900°C. Synthesis was then carried out using CH_4/N_2 (gas flow ratio = 1 : 4) plasma at 800 W for a duration of 60 s. The samples were allowed to cool under a constant N_2 flow. The conditions used were similar to the ones reported in our previous publications[59–62]. The hydrogen microwave plasma treatment of the FLG was carried out at three different substrate temperatures of 50, 100 and 200°C at a chamber pressure of ~2 Torr with a treatment time of 90 s, and microwave power of 150 W.

Characterizations. Raman spectroscopy was performed using an ISA LabRam system equipped with a 632.8 nm He-Ne laser with a spot size of approximately 2–3 μm, yielding a spectral resolution of better than 2 cm^{-1}. Due care was given to minimize sample heating by using a low laser power below 2 mW. The XPS spectrum was measured on a Kratos Axis Ultra DLD employing an Al Kα radiation (1486.6 eV). The X-ray absorption near edge structure (XANES) spectra was obtained using the high-energy spherical grating monochromator 20A-beamline at the National Synchrotron Radiation Research Center (NSRRC), Hsinchu, Taiwan. XES and corresponding C K-edge XANES measurements were carried out at beamline-7.0.1 at the Advanced Light Source, Lawrence Berkeley National Laboratory. The energy resolutions of XES and XANES measurements were ~0.35 and 0.1 eV, respectively. The magnetic properties of these samples were characterized by a SQUID-type magnetometer with sensitivity better than 5×10^{-8} emu. The topographical and magnetic force microscopy (MFM) measurements were carried out using a Veeco Dimension 3100 AFM connected to a Nanoscope IIIa controller in a tapping mode configuration. To detect magnetic domains in the prepared samples, low moment magnetic probes with Co/Cr coatings were used. To assess the correlation of surface features and assess the effects of magnetization, the topographical (height), amplitude and phase signals were imaged simultaneously for both conventional topographical imaging and magnetic measurements. MFM data were acquired while maintaining a constant lift scan height of ~10 nm above the topography (height) data to reduce coupling between Van der Waals and magnetic forces and also to demonstrate the field strength generated by the magnetic domains. In addition, the electron field emissions (EFEs) were measured using a Keithley power supply.

1. Novoselov, K. S. *et al.* Electric field effect in atomically thin carbon films. *Science* **306**, 666–669 (2004).
2. Geim, A. K. Graphene: Status and Prospects. *Science* **324**, 1530–1534 (2009).
3. Gass, M. H. *et al.* Free-standing graphene at atomic resolution. *Nature Nanotech.* **3**, 676–681 (2008).
4. Stankovich, S. *et al.* Graphene-based composite materials. *Nature Lett.* **442**, 282–286 (2006).
5. Li, L. *et al.* Functionalized graphene for high-performance two-dimensional spintronics devices. *ACS Nano* **5**, 2601–2610 (2011).
6. Hong, A. J. *et al.* Graphene Flash Memory. *ACS Nano* **5**, 7812–7817 (2011).

7. Sofo, J. O., Chaudhari, A. S. & Barber, G. D. Graphane: A two-dimensional hydrocarbon. *Phys. Rev. B* **75**, 153401: 1–4 (2007).
8. Elias, D. C. *et al.* Control of Graphene's Properties by Reversible Hydrogenation: Evidence for Graphane. *Science* **323**, 610–613 (2009).
9. Zhou, J. *et al.* Ferromagnetism in Semihydrogenated Graphene Sheet. *Nano Lett.* **9**, 3867–3870 (2009).
10. Bostwick, A. *et al.* Quasiparticle Transformation during a Metal-Insulator Transition in Graphene. *Phys. Rev. Lett.* **103**, 056404: 1–4 (2009).
11. Haberer, D. *et al.* Tunable Band Gap in Hydrogenated Quasi-Free-Standing Graphene. *Nano letters* **10**, 3360–3366 (2010).
12. Guisinger, N. P. *et al.* Exposure of Epitaxial Graphene on SiC(0001) to Atomic Hydrogen. *Nano letters* **9**, 1462–1466 (2009).
13. Jørgensen, R. *et al.* Atomic Hydrogen Adsorbate Structures on Graphene. *J. Am. Chem. Soc* **131**, 8744–8745 (2009).
14. Zhou, J., Wang, Q., Sun, Q. & Jena, P. Stability and electronic structure of bilayer graphane. *Appl. Phys. Lett.* **98**, 063108: 1–3 (2011).
15. Balog, R. *et al.* Bandgap opening in graphene induced by patterned hydrogen adsorption. *Nature Mater.* **9**, 315–319 (2010).
16. Xie, L. *et al.* Room temperature ferromagnetism in partially hydrogenated epitaxial grapheme. *Appl. Phys. Lett.* **98**, 193113: 1–3 (2011).
17. Schmidt, M. J. & Loss, D. Edge states and enhanced spin-orbit interaction at graphene/graphane interfaces. *Phys. Rev. B* **81**, 165439: 1–12 (2010).
18. Ray, S. C. *et al.* Field emission effects of nitrogenated carbon nanotubes on chlorination and oxidation. *J. Appl. Phys.* **104**, 063710: 1–5 (2008).
19. Ferrari, A. C. *et al.* Raman Spectrum of Graphene and Graphene Layers. *Phys. Rev. Lett.* **97**, 187401: 1–4 (2006).
20. Ferrari, A. C. Raman spectroscopy of graphene and graphite: Disorder, electron–phonon coupling, doping and nonadiabatic effects. *Solid State Commun.* **143**, 47–57 (2007).
21. Tuinstra, F. & Koenig, J. L. Raman Spectrum of Graphite. *J. Chem. Phys.* **53**, 1126–1130 (1970).
22. Ferrari, A. C. & Robertson, J. Interpretation of Raman spectra of disordered and amorphous carbon. *Phys. Rev. B* **61**, 14095–14107 (2000).
23. Wu, W. *et al.* Control of thickness uniformity and grain size in graphene films for transparent conductive electrodes. *Nanotechnology* **23**, 035603: 1–10 (2012).
24. Wang, Y. Y. *et al.* Raman Studies of Monolayer Graphene: The Substrate Effect. *J. Phys. Chem. C* **112**, 10637–10640 (2008).
25. Ryu, S. *et al.* Reversible Basal Plane Hydrogenation of Graphene. *Nano Lett.* **8**, 4597–4602 (2008).
26. Graf, D. *et al.* Spatially Resolved Raman Spectroscopy of Single- and Few-Layer Graphene. *Nano Lett.* **7**, 238–242 (2007).
27. Xie, L., Jiao, L. & Dai, H. Selective etching of graphene edges by hydrogen plasma. *J. Am. Chem. Soc.* **132**, 14751–14753 (2010).
28. Luo, Z. *et al.* Thickness-Dependent Reversible Hydrogenation of Graphene Layers. *ACS Nano* **3**, 1781–1788 (2009).
29. Stohr, J. *NEXAFS Spectroscopy*, Springer-Verlag, Berlin 1991.
30. Hou, Z. *et al.* Effect of Hydrogen Termination on Carbon *K*-Edge X-ray Absorption Spectra of Nanographene. *J. Phys. Chem. C* **115**, 5392–5403 (2011).
31. Entani, S. *et al.* Growth of nanographite on Pt(111) and its edge state. *Appl. Phys. Lett.* **88**, 153126–153128 (2006).
32. Pacilé, D. *et al.* Near-Edge X-Ray Absorption Fine-Structure Investigation of Graphene. *Phys. Rev. Lett.* **101**, 066806: 1–4 (2006).
33. Hua, W., Gao, B., Li, S., Agren, H. & Luo, Y. X-ray absorption spectra of graphene from first-principles simulations. *Phys. Rev. B* **82**, 155433: 1–7 (2010).
34. Gao, H., Wang, L., Zhao, J., Ding, F. & Lu, J. Band Gap Tuning of Hydrogenated Graphene: H Coverage and Configuration Dependence. *J. Phys. Chem. C* **115**, 3236–3242 (2011).
35. Chiou, J. W. *et al.* Nitrogen-Functionalized Graphene Nanoflakes (GNFs:N): Tunable Photoluminescence and Electronic Structures. *J. Phys. Chem. C* **116**, 16251–16258 (2012).
36. Shkrebtii, A. I. *et al.* Graphene and graphane functionalization with hydrogen: electronic and optical signatures. *Phys. Status Solidi C* **9**, 1378–1383 (2012).
37. Bunch, J. S. *et al.* Impermeable Atomic Membranes from Graphene Sheets. *Nano letters* **8**, 2458–2462 (2008).
38. Zhou, Y. G., Zu, X. T., Gao, F., Nie, J. L. & Xiao, H. Y. Adsorption of hydrogen on boron-doped graphene: A first-principles prediction. *J. Appl. Phys.* **105**, 014309: 1–4 (2009).
39. Matte, H. R., Subrahmanyam, K. S. & Rao, C. N. R. Novel Magnetic Properties of Graphene: Presence of both Ferromagnetic and Antiferromagnetic Features and Other Aspects. *J. Phys. Chem. C* **113**, 9982–9985 (2009).
40. Yang, H. X., Chshiev, M., Boukhvalov, D. W., Waintal, X. & Roche, S. Inducing and optimizing magnetism in graphene nanomeshes. *Phys. Rev. B* **84**, 214404: 1–7 (2011).
41. Rout, C. S., Kumar, A., Kumar, N., Sundaresan, A. & Fisher, T. S. Room-temperature ferromagnetism in graphitic petal arrays. *Nanoscale* **3**, 900–903 (2011).
42. Ning, G. *et al.* Ferromagnetism in nanomesh grapheme. *Carbon* **51**, 390–396 (2013).
43. Yazyev, O. V. & Helm, L. Defect-induced magnetism in grapheme. *Phys. Rev. B* **75**, 25408–125412 (2007).
44. Zhou, J., Wu, M. M., Zhou, X. & Sun, Q. Tuning electronic and magnetic properties of graphene by surface modification. *Appl. Phys. Lett.* **95**, 103108 (2009).
45. Zhou, J. & Sun, Q. How to fabricate a semihydrogenated graphene sheet? A promising strategy explored. *Appl. Phys. Lett.* **101**, 073114 (2012).
46. Eng, A. Y. S. *et al.* Searching for Magnetism in Hydrogenated Graphene: Using Highly Hydrogenated Graphene Prepared via Birch Reduction of Graphite Oxides. *ACS Nano* **7**, 5930–5939 (2013).
47. Pumera, M. & Wong, C. H. A. Graphane and hydrogenated graphene. *Chem. Soc. Rev.* **42**, 5987–5995 (2013).
48. Subrahmanyam, K. S. *et al.* Chemical storage of hydrogen in few-layer graphene. *P. Natl. Acad. Sci.* **108**, 2674–2677 (2011).
49. Wang, Y. *et al.* Toward high throughput interconvertible graphane-to-graphene growth and patterning. *ACS nano* **4**, 6146–6152 (2010).
50. Burgess, J. S. *et al.* Tuning the electronic properties of graphene by hydrogenation in a plasma enhanced chemical vapor deposition reactor. *Carbon* **49**, 4420–4426 (2011).
51. Yuan, G. D. *et al.* "Graphene sheets via microwave chemical vapor deposition." *Chem. Phys. Lett.* **467**, 361–364 (2009).
52. Wang, Y. *et al.* Room-Temperature Ferromagnetism of Graphene. *Nano Lett.* **9**, 220–224 (2009).
53. Lee, H., Son, Y. W., Park, N., Han, S. & Yu, J. Magnetic ordering at the edges of graphitic fragments: Magnetic tail interactions between the edge-localized states. *Phys. Rev. B* **72**, 174431–174438 (2005).
54. Berashevich, J. & Chakraborty, T. Tunable band gap and magnetic ordering by adsorption of molecules on grapheme. *Phys. Rev. B* **80**, 033404–033407 (2009).
55. Lehtinen, P. O., Foster, A. S., Ma, Y., Krasheninnikov, A. V. & Nieminen, R. M. Irradiation-Induced Magnetism in Graphite: A Density Functional Study. *Phys. Rev. Lett.* **93**, 187202–187205 (2004).
56. Harigaya, K. The mechanism of magnetism in stacked nanographite: theoretical study. *J. Phys.: Condens. Matter* **13**, 1295–1302 (2001).
57. Esquinazi, P. *et al.* Induced Magnetic Ordering by Proton Irradiation in Graphite. *Phys. Rev. Lett.* **91**, 227201–227204 (2003).
58. Han, K. H., Spemann, D., Esquinazi, P., Höhne, R. V. R. & Butz, T. Ferromagnetic Spots in Graphite Produced by Proton Irradiation. *Adv. Mater.* **15**, 1719–1722 (2003).
59. Soin, N. *et al.* Exploring the fundamental effects of deposition time on the microstructure of graphene nanoflakes by Raman scattering and X-ray diffraction. *Cryst. Eng. Comm* **13**, 312–318 (2011).
60. Soin, N., Roy, S. S., Mitra, S. K., Thundat, T. & McLaughlin, J. A. Nanocrystalline ruthenium oxide dispersed Few Layered Graphene (FLG) nanoflakes as supercapacitor electrodes. *J. Mater. Chem.* **22**, 14944–14950 (2012).
61. Soin, N. *et al.* Enhanced and Stable Field Emission from in Situ Nitrogen-Doped Few-Layered Graphene Nanoflakes. *J. Phys. Chem. C* **115**, 5366–5372 (2011).
62. Soin, N., Roy, S. S., Sharma, S., Thundat, T. & McLaughlin, J. A. Electrochemical and oxygen reduction properties of pristine and nitrogen-doped few layered graphene nanoflakes (FLGs). *J. Solid State Electrochem.* **17**, 2139–2149 (2013).

Acknowledgments

Author contributions

S.C.R. designed the experiments with the initial discussion with N.S. and S.S. Roy. The FLGs are synthesised by N.S. The magnetic experiments were designed by A.M.S. and performed by S.K.G. and T.M. The XES and XANES data were designed by W.F.P. and collected by C.H.C. The data were analyzed and the manuscript prepared by S.C.R. All authors discussed the results and contributed to finalization of the manuscript.

Additional information